Experimental demonstration of plasmon-soliton coupling

TINTU KURIAKOSE[1], GILLES RENVERSEZ[2*], VIRGINIE NAZABAL[3,4], MAHMOUD ELSAWY[2], TOMAS HALENKOVIC[4], PETR NEMEC[4], MATHIEU CHAUVET[1*]

[1] FEMTO-ST Institute, UMR CNRS 6174, University of Bourgogne Franche-Comté, 15B avenue des Montboucons, 25030 Besançon, France
[2] University of Aix-Marseille, CNRS, Centrale Marseille, Institut Fresnel, Marseille 13013, France
[3] Institut des sciences chimiques de Rennes, UMR CNRS 6226, Equipe Verres et Céramiques, Université de Rennes 1, 35042 Rennes, France
[4] Department of Graphic Arts and Photophysics, Faculty of chemical Technology, University of Pardubice, Studentská 573, 53210 Pardubice, Czech Republic

Corresponding authors: mathieu.chauvet@univ-fcomte.fr; gilles.renversez@univ-amu.fr

We report the experimental observation of plasmon-soliton coupling. The demonstration is performed in a chalcogenide-based four-layer planar geometry designed to limit plasmon propagation losses while exhibiting efficient Kerr self-focusing at moderate power. The observations reveal a strongly enhanced self-focusing undergone by a self-trapped beam propagating inside the structure. As expected, only TM polarized waves exhibit such a behavior. Different experimental arrangements are tested that unambiguously reveal the nonlinear plasmon-soliton coupling which is corroborated by numerical simulations.

OCIS codes: *(190.0190)* Nonlinear optics*, (250.5403) Plasmonics, (240.6680) Surface plasmons, (190.3270) Kerr effect, (190.6135) Spatial solitons, (230.7400) Waveguides, slab*

The efficiency of nonlinear optical processes is well known to benefit from extreme light confinement. One-way to form such strong electromagnetic field is to exploit light interactions with metal nanostructures. The surface plasmon polariton (SPP) [1] at a metal-dielectric interface, associated with both a collective oscillation of free charges in the metal and an extremely confined electromagnetic wave, is one of most the emblematic discovery. Since then plasmonics has evolved as a flourishing research field [2]. Merging the fields of plasmonics and nonlinear optics to exploit these intense optical fields comes logically and let envision a variety of fascinating and original physical phenomena along with great potential. In addition to providing enhanced nonlinear effects with ultrafast response times, plasmonic nanostructures allow nonlinear optical components to be scaled down in size. As a consequence, nonlinear plasmonics [3] is a field of research that has been growing over the past years with applications such as frequency conversion [4], switching and modulation [5]. However, this field of research is still in its infancy.

More specifically, first descriptions of one-dimensional nonlinear plasmon–soliton and nonlinear surface waves at metal/dielectric and dielectric/dielectric interfaces were unveiled in the early eighties [6–9]. The concept being to propagate a plasmon polariton wave at a metal-nonlinear material interface in order to induce an exalted Kerr self-focusing effect that give rise to a self-trapped wave. Up to now the problem has been tackled only theoretically, based on analytical and numerical calculations [10–20] dealing with both spatial and temporal beam trapping. Despite this constant and comprehensive development on modelling, up to now, no experimental evidence of self-trapped nonlinear plasmonic wave has yet been revealed.

Among the practical challenges inherent to this plasmon assisted self-focusing demonstration is the large propagation losses associated with plasmons, the request for a strong Kerr coefficient and the damage threshold intensity of the plasmonic structure.

In the present work, a four-layer slab component is designed and fabricated to support a moderate loss SPP along with strong Kerr nonlinear effects. The first experimental observation of a hybrid coupling between a spatial soliton and a SPP is performed in this structure. It reveals a giant enhancement of the beam self-trapping efficiency due to the plasmonic effect.

The content of the article is as follows: in a first part we describe the structure design and fabrication steps. Secondly, nonlinear optical characterizations are presented. Finally, numerical simulations are confronted to the experiments and results are discussed.

Design and fabrication of the structures

The origin of our nonlinear plasmonic component is a planar chalcogenide waveguide that possesses the suitable nonlinear properties to form Kerr spatial solitons at near infrared wavelengths as demonstrated in refs [21,22]. For the propagating wave to generate a SPP a metal film must be present at the top surface. However, a compromise has to be found between a tight light confinement provided by the plasmonic effect, which we want to exploit to efficiently exalt the Kerr effect, and the propagation losses that can be too high and prevent the observation of the Kerr self-focusing. The chosen solution is to insert a thin low refractive index dielectric layer in between the metal

and the nonlinear dielectric layer. The designed structure derives from our previously published theoretical studies [13,14]. For TM polarization, the studied architecture supports a plasmonic wave that extends in the nonlinear dielectric layer. Therefore, propagation losses are weaker compared to the case of the extremely confined plasmonic waves present at a basic metal-dielectric interface. For our multilayer structure we expect plasmon

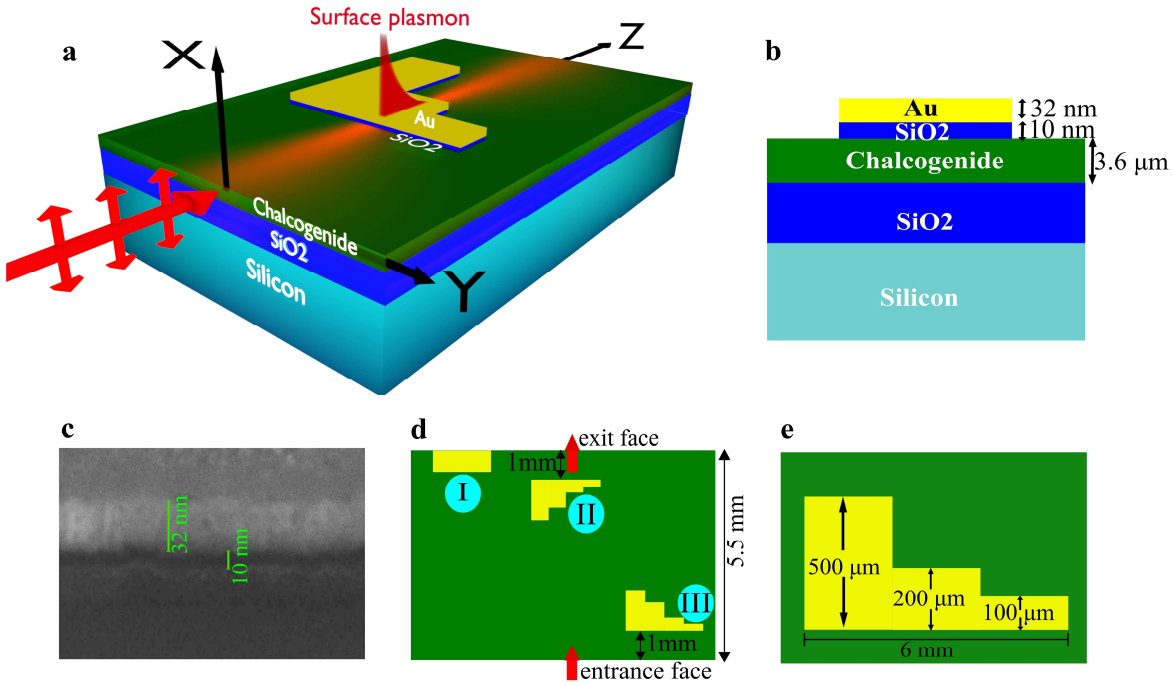

Fig. 1: a, artistic 3-D view of the experiment. b, schematic description of the cross section of the sample with the plasmonic structure. c, SEM image of the Au/ SiO_2/ chalcogenide interfaces. d, schematic overall top view of the sample showing the three studied configurations denoted by I, II and III. e, detailed top view of a staircase metallic pattern.

propagation over few hundreds micrometers. In addition, the plasmonic tail present in the nonlinear layer will efficiently activate the Kerr effect. This configuration is thus favorable to reveal the formation of a self-focused beam that takes advantage of the plasmon-enhanced Kerr effect.

To be more specific the Kerr layer is constituted of a 3.6 µm thick $Ge_{28.1}Sb_{6.3}Se_{65.6}$ chalcogenide glass deposited by RF magnetron sputtering on an oxidized silicon wafer [23] as shown in Fig.1. This glass composition was chosen due to its large Kerr nonlinearity ($n_2 = 5.5x10^{-18}$ m^2/W), moderate two-photon absorption coefficient ($\alpha_2 =$ 0.43 cm/GW) at the wavelength of interest of 1.55 µm and a high damage threshold intensity evaluated to 2 GW/cm^2 [22]. In addition, this film composition presents a lower photosensitivity than glasses with higher antimony content [24]. The chalcogenide refractive index at 1.55 µm is 2.54. A silica buffer layer followed by a gold layer are then deposited by the sputtering technique. Finite Element Method (FEM) numerical simulations [25,26] have been performed to compute the nonlinear modes in the structure in order determine the optimum thicknesses for these top layers. It shows that the silica thickness is the most critical parameter for the design as expected from a previous study [27].

As depicted in Fig. 2a, for a silica layer thickness thicker than 25 nm TM and TE vertical (along the X-axis) profiles of fundamental propagating modes are very similar. The presence of the metal marginally influences their distribution as witnessed by the calculated profiles very similar to the one of the fundamental guided modes of the SiO_2/chalcogenide slab waveguide. To the contrary, when we consider a thinner SiO_2 layer the TM wave is strongly affected by the metal and its plasmonic nature is obvious with a strong localization at the metal/dielectric interface as illustrated in Fig. 2b for the case of a 5 nm thick SiO_2 layer. Note the TE mode (Fig. 2b) does not present such characteristics due to the absence of any electric field component perpendicular to the metal interface. As a compromise between electric field enhancement and propagation losses, we opt for the fabrication of a plasmonic structure with a 10 nm thick SiO_2 buffer layer. Also, note that the deposition of a thinner SiO_2 layer of good quality is very challenging with the operated sputtering deposition technique. Finally, a 32 nm thick gold layer was then sputtered on top to form the designed plasmonic structure (PS), as illustrated in Fig. 1b. A cross section of the fabricated structure was analyzed by SEM (Fig. 1c) which confirms that the targeted and fabricated nanolayer thicknesses are in accordance. As depicted in Fig. 1d, the gold layer is not present on the whole surface of the chalcogenide waveguide. The gold layer is instead patterned to obtain either a rectangular or staircase (Fig. 1e) PS. This arrangement provides the versatility to analyze several configurations by choosing the position along the Y-axis of the launched beam. Propagation without the PS is tested as a reference and is then compared with observations performed for different PS lengths *h* and locations along propagation.

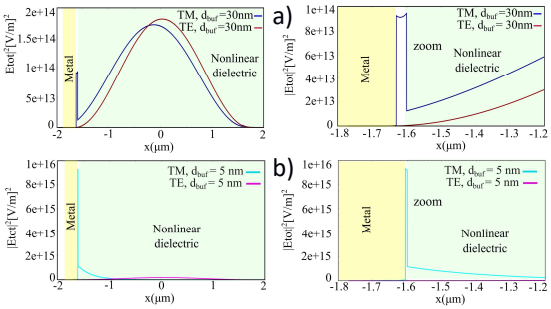

Fig. 2: calculated fundamental TM and TE mode profiles along the X-axis for SiO_2 buffer thickness h equal to 30 nm (a) and 5 nm (b).

Specifically, three different PS locations are considered as described in figure 1d. The first one is a rectangular plasmonic pattern, h = 660 µm long, located at the exit face of the sample (configuration I). The two other configurations correspond to staircase PS with h varying from 100 µm to 500 µm, present either 1 mm before the exit face or 1mm after the entrance face to form configurations II and III, respectively. Input and output faces of the 5.5 mm long sample are formed by cleaving the processed wafer.

Optical characterizations

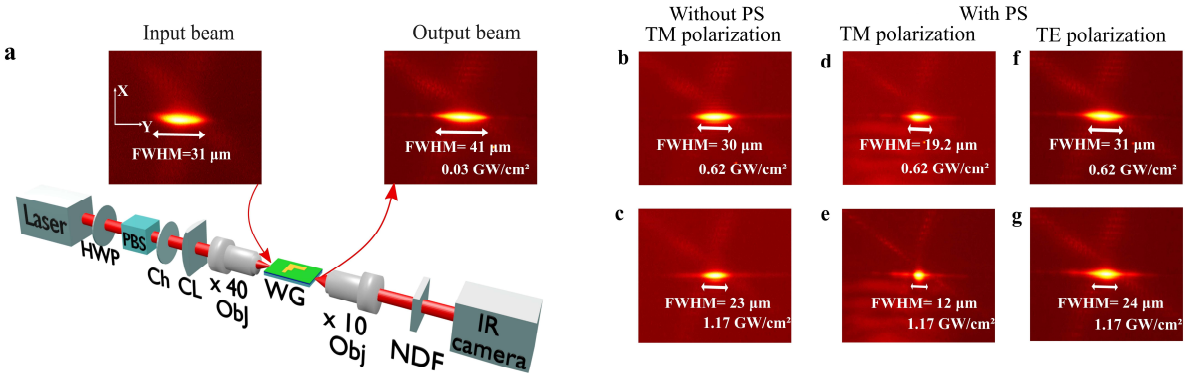

Fig. 2: a, Experimental setup used for the observation of plasmon-soliton coupling and intensity distribution of the injected and output beam in linear regime. HWP; half wave plate, PBS; polarizing beam splitter, Ch; chopper, CL; cylindrical lens, Obj; microscope objective, NDF; neutral density filters. b-g, Intensity distribution of self-focused output beams for two input intensities without PS (b, c), with PS corresponding to configuration I for TM polarization (d, e) and for TE polarization (f, g).

Optical measurements are performed with an optical parametric oscillator emitting 200 fs pulses at a repetition rate of 80 MHz at 1550 nm (Chameleon OPO from Coherent) as shown in Fig. 3a. The power is varied by the combination of a half wave plate and a polarizer. The latter component is also used to adjust the polarization state of the injected beam to TM or TE polarization. An optical chopper can also be inserted to change the average power. The laser beam is shaped into an elliptical spot using a cylindrical lens and a x40 microscope objective to form 4µm and 31µm (Fig. 3a) beam waists (FWHM) along X-axis and Y-axis, respectively. The beam is end-fire coupled into the waveguide so that the 31µm beam waist is located 2 mm inside the sample. Such an arrangement lower the intensity at the entrance face compare to the intensity inside the waveguide. It thus helps to prevent input facet damage at high intensity regime. In addition, it gives a weakly diffracting beam over the 5.5 mm long propagation distance. Careful beam alignment is also performed to maximize the beam overlap with the fundamental guided mode of the planar waveguide and thus avoid excitation of higher order modes. The beam profile at the output of the sample is imaged on a vidicon camera with a x10 microscope objective. It confirms that higher order modes are negligible in the propagating light. Input and output powers are monitored by power meters to deduce the coupling efficiency and the waveguide transmission. After 5.5 mm propagation inside the waveguide, the diffracted beam reaches a 41 µm FWHM along Y-axis (Fig. 3a) in linear regime (low intensity). In this regime a ~21% waveguide transmission is measured for both TM and TE polarizations when light propagates away from the metallized area. This transmitted power is consistent with a coupling efficiency of 28% and propagation losses of about 0.19 cm^{-1}. The input spatial averaged incident intensity is determined by dividing the coupled light peak power by the elliptical section of the guided mode at the entrance face corresponding having waists of 1.21 µm along X-axis and 30µm (35.5µm FWHM) along Y-axis.

To unambiguously reveal the influence of the SPP on the beam self-focusing, we first characterize the self-trapping behavior in the absence of metallic layer along the beam path. These preliminary experiments can thus be considered as a reference. As shown in references [21,22] the optical Kerr nonlinearity in such chalcogenide slab waveguides can support spatial solitons at near-infrared wavelengths. In the tested sample we observe that, for an input intensity of 0.62 GW/cm^2, a 30 µm FWHM beam is obtained at the output face (Fig. 3b). This size is close to the injected beam waist of 31 µm (Fig. 3a) which indicates that diffraction is compensated by the nonlinear Kerr self-focusing effect to form a spatial soliton. If the input intensity is further raised a stronger focusing effect occurs. For an intensity of 1.17 GW/cm^2 a 23 µm FWHM is obtained at the output (Fig. 3c). Note that the very same behavior is observed for both TM and TE polarizations for this configuration without PS.

We then shift laterally the sample so that a PS is present on the trajectory of the launched beam. To be more

specific, configuration I described in Fig. 1d is first considered with a PS length *h* of 660 µm. In linear regime the presence of this metallic structure located near the end of the waveguide does not modify the observed output beam distribution. The linear transmission is however reduced due to additional propagation losses compared to the situation without the PS. We deduce that under the PS the attenuation is 0.57 cm^{-1} and 28 cm^{-1} for TE and TM polarized light, respectively. The large attenuation for the TM case is a first indication of the plasmonic effect predicted in Fig. 2. Subsequently, as the intensity is raised, a strong enhancement of the self-focusing behavior is observed at the output of the waveguide for TM waves. For instance, for an input intensity of 0.62 GW/cm^2 (Fig. 3d) the output beam is already narrower (19 µm FWHM) than the injected one (31 µm FWHM) while a higher input intensity of 1.17 GW/cm^2 leads to a very efficient trapping of the beam as witnessed by the output beam of 12 µm FWHM (Fig. 3e). By comparing this result with the one obtained at the same intensity without PS (Fig. 3c) we can deduce that the plasmonic enhanced nonlinear effect focuses the beam from about 23 µm to 12 µm FWHM over the 660 µm long structure. It is important to note that the exalted focusing is not observed for the TE polarization. Indeed, as shown in Fig. 3 f, g, the TE mode shows no improved self-focusing compared to the configuration without the PS (Fig. 3 b, c). This polarization dependent behavior is a characteristic feature of the plasmonic effect. To exclude the possible influence of a thermally induced self-focusing the experiment was repeated by inserting a mechanical chopper after the light source that diminishes the average power to 40% while keeping the same peak power. We did not notice a measurable change compare to the behavior described in Fig. 3 that excludes any significant role of the temperature (data not shown).

First, the focusing effect takes place at a faster pace for low intensity. Second, about three times less intensity is needed to reach a 31µm output soliton beam compare to the case without plasmon. In addition, the FWHM evolves with a nonlinear trend and tends to saturate to a beam size approaching the narrow 11µm value at high intensity.

To get a better understanding of the disclosed plasmon-soliton coupling and the associated strongly enhanced focusing present for TM waves additional configurations are tested. We first studied the influence of the position of the PS along propagation. Fig. 4b compares the observed FWHM as a function of intensity for a 500 µm long plasmonic structure positioned either 1mm before the exit face (Fig. 1d conf. II) or 1 mm after the input face (Fig. 1d conf. III) and the previously described case of the 660 µm long PS located at the exit face. At very low intensity the beam undergoes the same free diffraction in the 5.5 mm long sample regardless of the PS location which precludes any linear beam distortion from the PS. As soon as the intensity is raised the output beam sharply focuses in accordance with the Kerr-lens effect present in the PS. However, when the intensity is increased above an intensity threshold a spreading of the FWHM beam is observed for PS located before the output face. The threshold is about 0.35 GW/cm^2 and 0.87 GW/cm^2 for a PS positioned 1 mm after the entrance face (conf. III) or 1 mm before the exit face (conf. II), respectively. This behavior can once again be explained by the strong localized self-focusing induced by the PS. Indeed, when such a focusing leads to a narrow spot the beam diffraction cannot be compensated anymore by the weaker nonlinearity present after the PS and the beam diffraction is dominant. Consequently, beam spreading is observed at the output face. The diffraction is weaker in configuration II since the PS is only 1 mm from the output observation

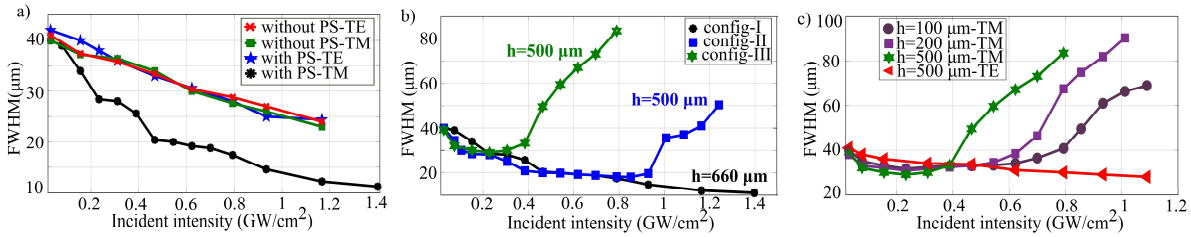

Fig. 4 : a, measured output beam FWHM as a function of input intensity for both TM and TE polarizations without PS and with a PS corresponding to configuration I. b, evolution of output beam width as a function of input intensity for configurations I, II and III for TM polarization. c, evolution of output beam width for configuration III for PS lengths h of 500 µm, 200 µm and 100 µm for TM polarization and for h of 500µm for TE polarization.

The experimentally demonstrated striking self-focusing enhancement due to the plasmonic effect is also evident in the graph from Fig. 4a where the measured output FWHM beam is plotted as a function of the beam intensity for TE and TM polarizations both with and without the PS. For the three arrangements for which plasmon generation is not achievable, i.e. without PS or with PS for TE polarization, a similar behavior is observed. It is characterized by a gradual focusing with a linear evolution of the beam width versus intensity. The behaviour for a TM polarized mode in presence of a PS differs significantly. We first observe that this plasmon-enhanced configuration always gives rise to an output FWHM beam smaller than for the other three standard configurations. face. Note that, as observed experimentally, the input threshold intensity is expected to be weaker when the PS is close to the entrance face. Indeed, due to the linear and two photon absorptions, the intensity reaching the PS is not reduced as much as in configuration III where the PS is far from the input face.

To analyze the impact of the length h of the PS on the enhanced self-focusing observed for TM waves, experiments have also been conducted for PS lengths of 100 µm and 200 µm for configuration III (Fig. 1d-e). The results are presented in Fig. 4c along with measurements made with h = 500 µm and for the enhancement free TE polarization. As the intensity increases, the PS self-focusing enhancement focuses the beam to a minimum

value before spreading of the FWHM occurs. The shorter is the PS, the weaker is the nonlinear focusing effect. The minimum beam size is reached at an intensity of about 0.24 GW/cm^2, it gives an output FWHM of 31.6 µm, 30.7 µm and 29 µm for 100 µm, 200 µm and 500 µm PS length, respectively. As the intensity is further increased, the improved confinement brought by the PS gradually diminishes until the threshold intensity is reached which is characterized by the sudden defocusing. This threshold intensity raises as the PS length is reduced. It is a hint showing that even PS as short as 100µm can induce extreme focusing.

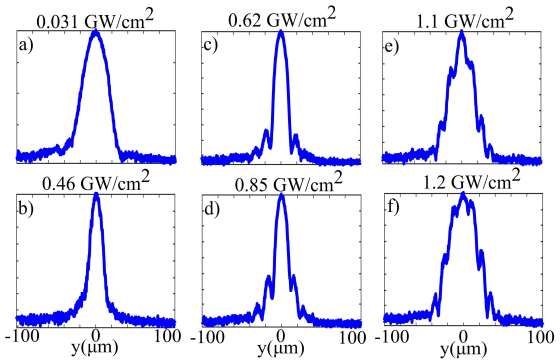

Fig 5 : Output beam profile evolution as a function of incident intensity for configuration II, TM polarization, h=500 µm.

Analysis of the output beam profile provides crucial additional information on the strong nonlinearity seen by the propagating beam that was not revealed by the FWHM measurements. In Fig. 5 the output beam profile is plotted for 6 intensity values for a 500 µm long PS positioned 1 mm from the output face (conf. II). The previously described efficient focusing effect first form a smooth profile beam with a weak pedestal (Fig. 5b). This beam then enlarges and develops symmetric side lobes on both sides of the main peak as the intensity is raised (Fig. 5). This unexpected behavior is corroborated by numerical calculations presented in the following section.

Simulations-Discussion

In order to confirm the role of the PS on the beam propagation in the PS and to gain insight into the observed phenomena we built a numerical model based on the spatial nonlinear Schrödinger equation adapted to take into account the mode field evolution along X-axis. This scalar model describes the transverse field profile along the Y-axis and its evolution versus propagation along Z-axis [28]. The three different configurations (I, II, or III) including the different lengths *h* of the PS can be solved. The field dependency along the vertical X-axis does not explicitly appear in the model but is considered indirectly through the Z-dependent modal properties (effective nonlinearity and propagation constants) that appear in the nonlinear Schrödinger equation. These modal parameters are obtained from the finite element method (FEM) based study of the fundamental TE and TM modes associated with the different sections of the full structure [25,26]. Specifically, the effective nonlinearity is computed using several integrals of the computed modal field. Without PS, the field profiles of both TE and TM modes (Fig. 2a) and thus the associated modal parameters are nearly identical. To the contrary, in presence of a PS with a 10 nm thick SiO_2 layer, the propagation constants are slightly different (typically 1%) but more importantly the field profiles are radically different. This dissimilarity gives an eightfold enhancement of the effective nonlinearity parameter for the TM mode compared to the TE mode.

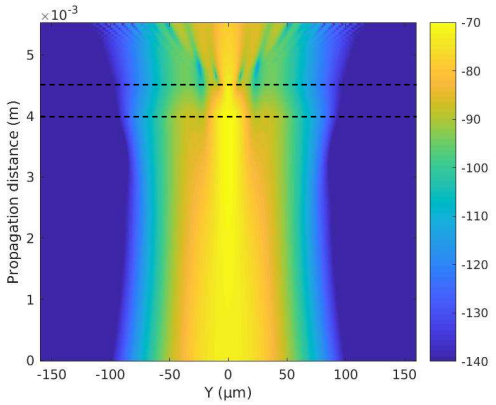

Fig. 6 : Color map in log scale of the beam intensity evolution along the Y-axis versus propagation inside the full structure for the TM polarization for configuration II with h = 500 µm in nonlinear regime (input peak intensity of 2.5 GW/cm²). The dashed lines represent the limits of the PS.

Fig. 6 presents the calculated evolution of the beam intensity along the Y-axis versus propagation inside the full structure for the TM polarization for configuration II with h = 500 µm at an input intensity (peak intensity I_{peak}=2.5 GW/cm^2) that corresponds to the experimental test in Fig. 5f. This emblematic case reveals several remarkable characteristics that give more insight to the behavior unveiled experimentally. First, we clearly see that the beam self-focuses along the first 2 mm then it becomes nearly invariant before converging dramatically to a highly focused central peak as it travels in the 500 µm long PS region indicated by the dashed lines. Finally, as the beam leaves this highly nonlinear PS region, diffraction overpass the self-focusing effect. It is important to note that the numerical model also predicts the symmetric lateral peaks observed experimentally in Fig. 5. These peaks are generated in the last part of the PS for intensity above 0.6 GW/cm^2 that is in fair agreement with the experiments. Spatial modulation instability can be at the origin of the beam break-up of an initial noisy broad beam propagating in Kerr nonlinear media but it does not fit to the present phenomena. First, the measured intensity dependence of the generated spatial frequency does not follow the scaling law of modulation instability [29,30]. Moreover, large amplitude spatial noise added in the present simulations do not give rise to the observed multi-peaks unless the plasmon-enhanced nonlinearity is present. We think the here described phenomenon has a similar origin than the beam breakup induced at the interface between a low Kerr-type nonlinearity dielectric region and a high nonlinearity one described in references [31,32]. Our numerical method is then used to assess the FWHM evolution versus intensity observed for

configuration I (Fig. 4a). The calculated values presented in Fig. 7 clearly predict the enhanced self-focusing effect induced to a TM polarized beam in presence of the PS in qualitative accordance with the experiments.

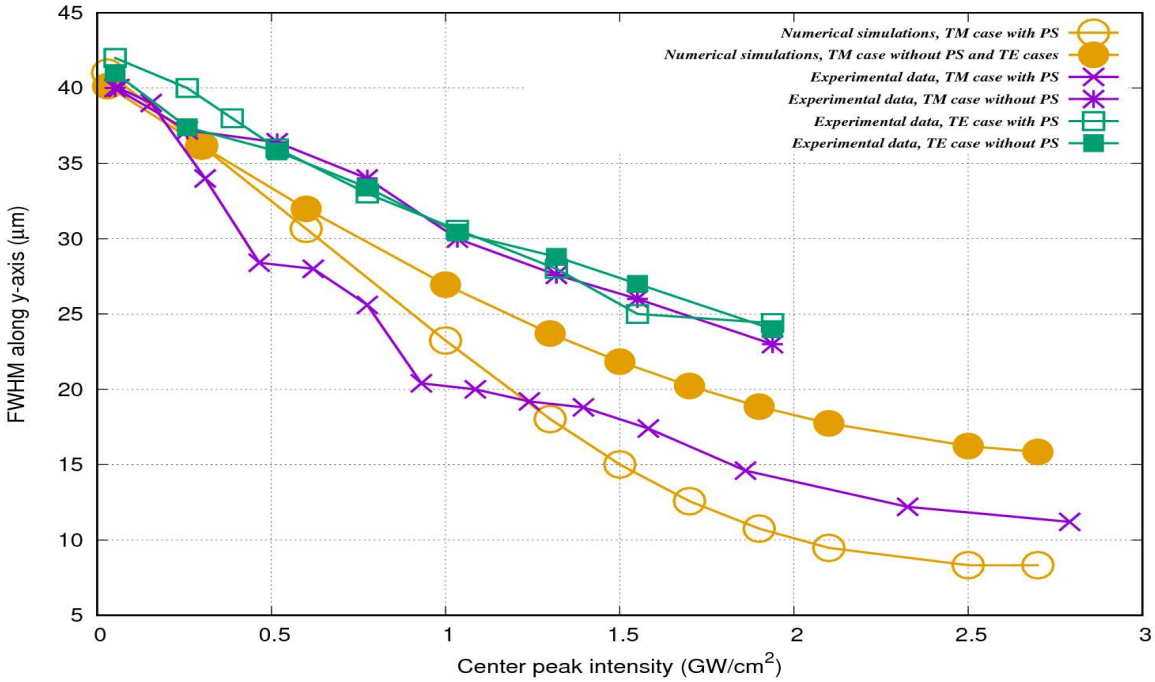

Figure 7 : Comparison of the computed and measured FWHM for configuration I as a function of the input peak intensity .

The saturation of the self-focusing effect appearing at high power is also observed in the simulations. Discrepancies between theory and experiments however remain with notably a stronger predicted focusing. First, some limitations of the model can be invoked: it is based on a scalar equation while the genuine problem is a vectorial one, paraxial approximations and calculation of the effective nonlinearity are not fully valid when beam profile rapidly transforms in the PS and the considered instantaneous response of the Kerr effect could be questioned in femtosecond regime [33]. At last, there is some uncertainty on the value of the n_2 and α_2 nonlinear coefficients of this uncommon chalcogenide composition [34]. Potential nonlinear effects present in the gold layer [35-37] can also be the reason of discrepancies between theory and measurements especially at high intensity regime.

Conclusion

In summary, a compelling spatial confinement of light observed only for TM polarization in a Kerr plasmonic structure arising from a plasmon-soliton coupling has been demonstrated experimentally. The designed structure consists of a slab waveguide made of a highly nonlinear chalcogenide waveguide covered with nanolayers of silica layer and gold. The thickness of the silica layer has been tailored to benefit from the enhance self-focusing due to the high-intensity plasmon while limiting the detrimental effect of propagation losses induced by the metal. Experimental observations are confirmed by numerical predictions obtained using an improved model of nonlinear propagation combining FEM modal results and spatial nonlinear Schrödinger equation. This first experimental proof validates the concept of the nonlinear spatial optical self-trapping enhanced by the assistance of a plasmon polariton. It also let envision the possibility to extend the demonstration to other nonlinear surface waves. In addition, the dramatic nonlinear beam reshaping induced over a distance of few hundreds microns at moderate light power also open up new perspectives for nonlinear integrated plasmonic devices.

Acknowledgements

The authors would like to acknowledge the financial support of the Region Franche-Comté and of Aix-Marseille University and of the Czech Science Foundation (project 16-17921S). This work was also partially supported by the FEMTO-ST MIMENTO technological facilities. We also thank Gwenn Ulliac for taking SEM image of the sample and Xavier Romain for the graphics help.

Author contributions

G.R. proposed the experiment. G.R., M.C. and T.K. designed the PS structure. V.N., P. N. and T.H. fabricated the samples. T.K. performed the optical characterizations. G.R. and M.E. conducted the simulations. T.K. assisted with the results analysis. M.C. and G.R. provided in-depth discussion of the project and analyzed the results. M.C., G.R. and T.K. wrote the manuscript.

References

1 S. L. Cunningham, A. A. Maradudin, and R. F. Wallis, "Effect of a charge layer on the surface-

plasmon-polariton dispersion curve," Phys. Rev. B **10**, 3342 (1974).
2 S. A. Maier, *Plasmonics: Fundamentals and Applications* (Springer, 2007).
3. M. Kauranen and A. V. Zayats, "Nonlinear plasmonics," Nat. Photonics **6**, 737 (2012).
4. H. J. Simon, D. E. Mitchell, and J. G. Watson, "Optical Second-Harmonic Generation with Surface Plasmons in Silver Films," Phys. Rev. Lett. **33**, 1531–1534 (1974).
5. M. Z. Alam, J. S. Aitchison, and M. Mojahedi, "A marriage of convenience: Hybridization of surface plasmon and dielectric waveguide modes," Laser Photonics Rev. **8**, 394–408 (2014).
6. V. M. Agranovich, V. Babichenko, and V. Y. Chernyak, "Nonlinear surface polaritons," JETP Lett **32**, 512–515 (1980).
7. W. J. Tomlinson, "Surface wave at a nonlinear interface," Opt. Lett. **5**, 323–325 (1980).
8. J. Ariyasu, C. T. Seaton, G. I. Stegeman, A. A. Maradudin, and R. F. Wallis, "Nonlinear surface polaritons guided by metal films," J. Appl. Phys. **58**, 2460–2466 (1985).
9. N. N. Akhmediev, "Novel class of nonlinear surface waves: asymmetric modes in a symmetric layered structure," Sov Phys JETP **56**, 299–303 (1982).
10. E. Feigenbaum and M. Orenstein, "Plasmon-soliton," Opt. Lett. **32**, 674–676 (2007).
11. A. R. Davoyan, I. V. Shadrivov, and Y. S. Kivshar, "Self-focusing and spatial plasmon-polariton solitons," Opt. Express **17**, 21732–21737 (2009).
12. K. Y. Bliokh, Y. P. Bliokh, and A. Ferrando, "Resonant plasmon-soliton interaction," Phys. Rev. A **79**, 041803 (2009).
13. W. Walasik, V. Nazabal, M. Chauvet, Y. Kartashov, and G. Renversez, "Low-power plasmon–soliton in realistic nonlinear planar structures," Opt. Lett. **37**, 4579–4581 (2012).
14. W. Walasik, G. Renversez, and Y. V. Kartashov, "Stationary plasmon-soliton waves in metal-dielectric nonlinear planar structures: Modeling and properties," Phys. Rev. A **89**, 023816 (2014).
15. W. Walasik and G. Renversez, "Plasmon-soliton waves in planar slot waveguides. I. Modeling," Phys. Rev. A **93**, 013825 (2016).
16. W. Walasik, G. Renversez, and F. Ye, "Plasmon-soliton waves in planar slot waveguides. II. Results for stationary waves and stability analysis," Phys. Rev. A **93**, 013826 (2016).
17. A. Marini and F. Biancalana, "Ultrashort Self-Induced Transparency Plasmon Solitons," Phys. Rev. Lett. **110**, 243901 (2013).
18. D. A. Smirnova, I. V. Shadrivov, A. I. Smirnov, and Y. S. Kivshar, "Dissipative plasmon-solitons in multilayer graphene", Laser Photonics Rev. 8, No. 2, 291–296 (2014)
19. M. L. Nesterov, J. Bravo-Abad, A. Nikitin, F. J. Garcia-Vidal, and L. Martin-Moreno, "Graphene supports the propagation of subwavelength opticals solitons", Laser Photonics Rev. 7, No. 2, L7–L11 (2013)
20. A. Pusch, I. V. Shadrivov, O. Hess, and Y. S. Kivshar, "Self-focusing of femtosecond surface plasmon polaritons," Opt. Express **21**, 1121–1127 (2013).
21. M. Chauvet, G. Fanjoux, K. P. Huy, V. Nazabal, F. Charpentier, T. Billeton, G. Boudebs, M. Cathelinaud, and S.-P. Gorza, "Kerr spatial solitons in chalcogenide waveguides," Opt. Lett. **34**, 1804–1806 (2009).
22. T. Kuriakose, E. Baudet, T. Halenkovič, M. M. R. Elsawy, P. Němec, V. Nazabal, G. Renversez, and M. Chauvet, "Measurement of ultrafast optical Kerr effect of Ge–Sb–Se chalcogenide slab waveguides by the beam self-trapping technique," Opt. Commun. **403**, 352–357 (2017).
23. V. Nazabal, F. Charpentier, J.-L. Adam, P. Nemec, H. Lhermite, M.-L. Brandily-Anne, J. Charrier, J.-P. Guin, and A. Moréac, "Sputtering and Pulsed Laser Deposition for Near- and Mid-Infrared Applications: A Comparative Study of Ge25Sb10S65 and Ge25Sb10Se65 Amorphous Thin Films: Sputtering and Pulsed Laser Deposition for Near- and Mid-IR Applications," Int. J. Appl. Ceram. Technol. **8**, 990–1000 (2011).
24. M. Olivier, J.C. Tchahame, P. Němec, M. Chauvet, V. Besse, C. Cassagne, G. Boudebs, G. Renversez, R. Boidin, E. Baudet, and V. Nazabal, "Structure, nonlinear properties, andphotosensitivity of (GeSe2)100-x(Sb2Se3)x glasses", Opt. Mat. Expr., **4**, 525-540 (2014).
25. M. M. R. Elsawy and G. Renversez, "Study of plasmonic slot waveguides with a nonlinear metamaterial core: semi-analytical and numerical methods", Journal of Optics, **19**, 075001 (2017).
26. M. M. R. Elsawy and G. Renversez, "Exact calculation of the nonlinear characteristics of 2D isotropic and anisotropic waveguides," Opt. Lett. **43**, 2446-2449 (2018).
27. M. M. R. Elsawy and G. Renversez, "Improved nonlinear slot waveguides using dielectric buffer layers: properties of TM waves", Opt. Lett., **41**, pp. 1542-1545 (2016).
28. S. Trillo and W. Torruellas (eds), Spatial Solitons, SSOS, volume 82, Springer 2001.
29. R. Malendevich, L. Jankovic, G. Stegeman, and J. S. Aitchison, "Spatial modulation instability in a Kerr slab waveguide," Opt. Lett. **26**, 1879–1881 (2001).
30. Y. Y. Lin, R. K. Lee, and Y. S. Kivshar, "Transverse instability of transverse-magnetic solitons and nonlinear surface plasmons," Opt. Lett. **34**, 2982–2984 (2009).
31. A. B. Aceves, J. V. Moloney, and A. C. Newell. "Theory of light-beam propagation at nonlinear interfaces. II. Multiple-particle and multiple-interface extensions", Phys. Rev. A **39**, 1828 (1989).
32. J. Sánchez-Curto, P. Chamorro-Posada, and G. S. McDonald, "bright and black soliton splitting at nonlinear interfaces", Phys. Rev. A **85**, 013836 (2012).
33. C. Cambournac, H. Maillotte, E. Lantz, J. M. Dudley, M. Chauvet, "Spatiotemporal behavior of periodic arrays of spatial solitons in a planar waveguide with relaxing Kerr nonlinearity", J. Opt. Soc. Am. B, **19**, 574-585 (2002).

34. G. Boudebs, S. Cherukulappurath, H. Leblond, J. Troles, F. Smektala, F. Sanchez, “Experimental and theoretical study of higher-order nonlinearities in chalcogenide glasses”. Opt. Comm., 219, 427-433 (2003).
35. R. W. Boyd, Z. Shi, I. De Leon, “The third-order nonlinear optical susceptibility of gold”, Opt. Comm., 326, 74-79 (2014).
36. H. Qian, Y. Xiao, Z. Liu, “Giant Kerr response of ultrathin gold films from quantum size effect”, Nat. Commun. **7**, 13153 (2016).
37. A. Tuniz, S. Weidlich, M. A. Schmidt, “Effectively Single-Mode Self-Recovering Ultrafast Nonlinear Nanowire Surface Plasmons”, Phys. Rev. Appl. 9, 044012 (2018).